1 **Exploring the sources of light-absorbing carbonaceous aerosols by integrating observational**

2 **and modeling results: insights from Northeast China**

3 Yuan Cheng[1], Xu-bing Cao[1], Sheng-qiang Zhu[2], Zhi-qing Zhang[1], Jiu-meng Liu[1,*], Hong-liang

4 Zhang[2], Qiang Zhang[3] and Ke-bin He[4]

5 [1] State Key Laboratory of Urban Water Resource and Environment, School of Environment, Harbin

6 Institute of Technology, Harbin, 150090, China

7 [2] Department of Environmental Science and Engineering, Fudan University, Shanghai 200438,

8 China

9 [3] Ministry of Education Key Laboratory for Earth System Modeling, Department of Earth System

10 Science, Tsinghua University, Beijing, 100084, China

11 [4] State Key Joint Laboratory of Environment Simulation and Pollution Control, School of

12 Environment, Tsinghua University, Beijing, 100084, China

13 * Corresponding author. Jiu-meng Liu (jiumengliu@hit.edu.cn).

14 **Abstract**

15 Light-absorbing carbonaceous aerosols are important contributors to both air pollution and radiative

16 forcing. However, their abundances and sources are still subject to non-negligible uncertainties,

17 which are highly responsible for the frequently-identified discrepancies between the observed and

18 modeled results. In this study, we focused on elemental carbon (EC) and light-absorbing organic

19 carbon (i.e., BrC) in Northeast China, a new targeted region of the latest clean air actions in China.

20 Three campaigns were conducted during 2018–2021 in Harbin, covering distinct meteorological

21 conditions and emission features. Various analytical methods were first evaluated, and the mass

22 concentrations of both BrC and EC were validated. The validated BrC and EC measurement results

23 were then used for source apportionment, together with other species including tracers (e.g.,

24 levoglucosan). The observation-based results suggested that despite the frigid winter in Harbin, the

25 formation of secondary organic aerosol (SOA) was enhanced at high levels of relative humidity

26 (RH). This enhancement could also be captured by an air quality model incorporating heterogeneous

27   chemistry. However, the model failed to reproduce the observed abundances of SOA, with

28   significant underestimations regardless of RH levels. In addition, agricultural fires effectively

29   increased the observation-based primary organic carbon (POC) concentrations and POC to EC ratios.

30   Such roles of agricultural fires were not captured by the model, pointing to substantial

31   underestimation of open burning emissions by the inventory. This problem merits particular

32   attention for Northeast China, given its massive agricultural sector.

1. Introduction

Black carbon (BC) and light-absorbing organic carbon, i.e., brown carbon (BrC), are important

contributors to not only haze pollution but also positive radiative forcing (Bond et al., 2013; Laskin

et al., 2015). While their environmental effects are usually predicted by chemical transport and

radiative transfer models, field observational results are necessary to constrain their simulated

spatial distributions and temporal variations (Koch et al., 2009; Samset et al., 2014; Stohl et al.,

2015; Wang et al., 2018; Gao et al., 2022). For example, several studies suggested that to improve

the agreement between simulated and observed BC concentrations, the BC lifetime should be on

the lower end of those assumed in current models (e.g., Samset et al., 2014). However, the

observational data on both BC and BrC are still subject to considerable uncertainties, largely due to

the lack of reference material and method for both species (Baumgardner, et al., 2012; Petzold et al.,

2013; Lack et al., 2014).

The measurement techniques for BC mass typically fall into four categories, i.e., thermal-

optical (Chow et al., 2007; Cavalli et al., 2010), light absorption (Petzold et al., 2005), laser-induced

incandescence (LII; Schwartz et al., 2006) and aerosol mass spectrometric methods (Onasch et al.,

2012). These approaches are based on different measurement principles, depending on the targeted

properties of BC (Petzold et al., 2013). For example, in the thermal-optical method, a particle-laden

filter is heated in an inert (i.e., He) and oxidizing (i.e., He/O_2) atmosphere sequentially to volatilize

and combust the deposited carbonaceous components. BC typically evolves after organic matters

due to its higher thermal stability. In addition, BC is strongly light-absorbing and thus its evolution

could lead to a rapid increase of the filter transmittance signal, which is typically monitored in the

spectral range of red light. Then based on the evolution patterns of the carbon and transmittance

3

55 signals, BC mass could be determined as the amount of carbon evolving during a specific segment

56 of thermal-optical analysis (Cavalli et al., 2010). In addition to the thermal-optical method, BC mass

57 could also be determined based on the aerosol light absorption coefficient (in Mm^{-1}; Moosmüller et

58 al., 2009), carbon ion signals in a mass spectrum measured by a Soot Particle Aerosol Mass

59 Spectrometer (SP-AMS; Onasch et al., 2012), or the incandescent radiation emitted during fast

60 heating, boiling and evaporation of BC in a LII instrument (Moteki and Kondo, 2010). The

61 multitude of measurement principles result in considerable discrepancies in BC results among

62 different methods, and interestingly, the discrepancies were usually not constant even for the same

63 study (Buffaloe et al., 2014; Sharma et al., 2017; Corbin et al., 2019; Li et al., 2019; Pileci et al.,

64 2021; Tinorua et al., 2024). For example, results from the LII and thermal-optical methods were

65 found to show BC ratios varying between 0.5 and 1.2 for several background sites in Europe, with

66 unclear reasons for the variability in discrepancies (Pileci et al., 2021).

67   Similar to BC, different methods co-exist for the measurement of BrC. For example, BrC's

68 light absorption coefficient is usually determined based on extract of filter sample (Hecobian et al.,

69 2010) or total aerosol absorption (Yang et al., 2009). Different relationships have been identified

70 between the results from these two approaches, e.g., strong correlation and close agreement (Zeng

71 et al., 2022), moderate to strong correlations with considerable differences in the absolute values

72 (Kumar et al., 2018; Cheng et al., 2021b), and little correlation (Chen et al., 2022). However, factors

73 responsible for the inconsistent relationships remain poorly understood. In addition, the

74 measurement of BrC mass is also challenging. This is particularly the case for studies using organic

75 solvents (e.g., methanol) to extract or isolate BrC. A major difficulty is that the amount of BrC

76 dissolved in organic solvents could not be directly measured, whereas the indirect approaches are

77   still under debate regarding the possible artifacts (Yan et al., 2020).

78   Nonetheless, the measurement methods of BC and BrC require further refinements to provide

79   more robust constraints on the modelling results. Such efforts are especially necessary for China,

80   given its more complex emission sources compared to North America and Europe. Here we focus

81   on Harbin, a representative megacity in Northeast China. With the improvement of air quality in

82   other regions such as the North China Plain (Xiao et al., 2021; Wang et al., 2023b), Northeast China

83   was targeted by the national-level clean air policy for the first time in 2021 (State Council, 2021).

84   This policy, i.e., the *Circular on Further Promoting the Pollution Prevention and Control Battle*,

85   proposed an ambitious goal of eliminating heavy or severe air pollution events in Northeast China

86   and other key regions. In addition, Harbin will be hosting the 9th Asia Winter Games in February of

87   2025, which posed another motivation for cleaning the air in Northeast China. However, the

88   roadmap for air quality improvement was to some extent masked for Harbin as well as other cities

89   in Northeast China, given that the sources and formation mechanisms of haze pollution were far

90   from being well understood with limited studies (e.g., Zhang et al., 2020; Wu et al., 2020; Ning et

91   al., 2022).

92   This study aimed at understanding the sources of light absorbing carbon in Harbin, based on a

93   synthesis of field observation and air quality modeling. We started with the coordinated

94   determination of BrC and BC masses in filter samples, followed by source apportionment using the

95   validated observational results. Then we used the observation-based BrC and BC source attributions

96   to constrain the predictions by an air quality model, with focuses on the model vs. observation

97   discrepancies and the drivers at play. This study provided implications for further efforts to

98   understand the haze pollution in Northeast China, with respect to both the measurement and

99   simulation of carbonaceous aerosols.

100   **2. Methods**

101   **2.1 Field observation**

102   A total of 486 $PM_{2.5}$ samples (24-h integrated) were collected at an urban site in Harbin during

103   three recent campaigns (Table 1). The sampling was performed on the campus of Harbin Institute

104   of Technology, using a portable sampler (MiniVol; Airmetrics, OR, USA) operated at a flow rate of

105   5 L/min with quartz-fiber filters (Pall Corporation, NY, USA). For each sample, a half of the filter

106   was measured for water-soluble inorganic ions and levoglucosan, using a Dionex ion

107   chromatography system (ICS-5000^{+}; Thermo Fisher Scientific Inc., MA, USA). The other half was

108   cut into two punches for the determination of organic carbon (OC) and elemental carbon (EC, as a

109   measure of BC mass), using a thermal/optical carbon analyzer (DRI-2001; Atmoslytic Inc., CA,

110   USA). The first punch was measured directly, while the second punch was immersed in methanol

111   (Fisher Scientific Company L.L.C., NJ, USA) for an hour without stirring or sonication, dried in air

112   for another hour, and then analyzed. All the pairs of untreated and extracted punches were measured

113   deploying the IMRPOVE-A temperature protocol, with selected pairs also analyzed using NIOSH

114   (Table 1). In addition, wavelength-resolved light absorption coefficients (b_{abs}) of the methanol

115   extracts were quantified using a spectrophotometer (Ocean Optics Inc., FL, USA) coupled with a

116   2.5m long liquid waveguide capillary cell (LWCC; World Precision Instrument, FL, USA). Samples

117   strongly impacted by firework emissions (N = 2, 3 and 6 for the three campaigns, respectively)

118   during the Chinese New Year periods were not further investigated in this study. More details of the

119   field observations were presented in Cheng et al. (2021a and 2022).

120   **Table 1.** Summary of $PM_{2.5}$ samples involved in this study. *N* indicates the number of samples from
121   each campaign. For each sample, both the untreated and extracted punches were used for thermal-

122 optical analysis. $NP_{\text{IMPROVE-A}}$ indicates the number of punch pairs analyzed by the IMPROVE-A

123 temperature protocol. NP_{NIOSH} was defined similarly. The split of OC and EC was based on the

124 transmittance charring correction for both protocols.

Measurement period	Main features[a]	N	$NP_{\text{IMPROVE-A}}$	NP_{NIOSH}[b]
October 16, 2018–April 14, 2019	Fires in late winter	180	180	180
October 16, 2019–February 4, 2020[c]	Humid winter	112	112	73
October 17, 2020–April 30, 2021	Fires in April	194	194	86

125 [a] Main features of the campaigns were presented briefly in Figure S1, and described in detail in

126 Cheng et al. (2021a and 2022).

127 [b] The selection of samples analyzed by both protocols will be explained in detail in Section 3.2.

128 [c] The 2019–2010 campaign covered a relatively short period due to the lockdown policy associated

129 with the outbreak of COVID-19.

130 **2.2 Air quality modeling**

131 A revised Community Multi-scale Air Quality (CMAQ) model was used to simulate OC and

132 EC in Harbin. Compared to the original version (5.0.1), a major update of the revised model was

133 the addition of new pathways for secondary organic aerosol (SOA) production, i.e., photochemical

134 and heterogeneous oxidation of isoprene epoxydiols, methacrylic acid epoxide, glyoxal and

135 methylglyoxal (Ying et al., 2015). Previous studies suggested that the revised CMAQ could

136 generally reproduce the observed meteorological conditions and PM$_{2.5}$ concentrations on a national

137 scale in China (Hu et al., 2016a; Wang et al., 2020). However, the model performance remained

138 inconclusive for PM$_{2.5}$ compositions in specific regions. In this study, the modeling was performed

139 over East China with a horizontal resolution of 36×36 km for the 2020–2021 measurement period.

140 The simulation results were extracted for the grid cell where the sampling site is located at, and then

141 compared with the observational results.

142 **3. Results and discussions**

143 **3.1 Validation of BrC measurement results**

144 Extracting filter samples by methanol was a common approach to measure brown carbon.

145   While the light absorption by BrC could be readily determined using the methanol extracts, it

146   remains challenging to quantify the mass concentration of BrC, i.e., methanol-soluble OC (MSOC).

147   Unlike water-soluble OC (WSOC), the measurement of MSOC could not be directly done using a

148   Total Organic Carbon analyzer and instead required indirect methods. For example, a four-step

149   procedure was developed by Chen et al. (2017), including drying the methanol extract in a nitrogen

150   flow, re-dissolving the residues in a small amount of methanol (100 μL), spiking a pre-baked filter

151   punch (prepared for thermal-optical carbon analyzer) with a known volume of the new extract (20

152   μL), and measuring the total carbon (TC) in the spiked filter after drying as MSOC. A simpler

153   approach was to determine MSOC as the difference in OC (or TC) concentrations between the

154   untreated and extracted filter punches. This method was initially developed by Chen and Bond

155   (2010), with a substantial concern being the loss of insoluble carbon (e.g., EC) during extraction.

156   However, this artifact was difficult to evaluate, largely due to the lack of reference method for the

157   measurement of EC mass (Petzold et al., 2013).

158   In addition to EC mass, optical attenuation (ATN) retrieved from the carbon analyzer could be

159   an alternative criterion for estimating the extraction-induced loss of insoluble carbon. ATN was

160   calculated as $\ln(I_{final}/I_{initial})$, where $I_{initial}$ and I_{final} indicates filter transmittance signals (I) measured

161   at the beginning and end of thermal-optical analysis, respectively. $I_{initial}$ was lower than I_{final} mainly

162   due to the absorption by light-absorbing aerosols (e.g., EC and BrC) and scattering or more

163   specifically backward scattering (Petzold et al., 2005) by the deposited particles (e.g., inorganic ions

164   and non-absorbing OC). Given that I was monitored at a wavelength of 632 nm, only strongly-

165   absorbing BrC could influence $I_{initial}$ and thus ATN through absorption, while SOA could be

166   considered almost non-absorbing (Lambe et al., 2013; Liu et al., 2015, 2016a). Thus we suggest that

167 (i) decrease of ATN after extraction, if occurred, could be mainly attributed to three possible factors,

168 including loss of EC, removal of strongly-absorbing BrC and removal of scattering compounds such

169 as SOA and nitrate; and (ii) if ATN measured by the untreated and extracted filters (i.e., $ATN_{untreated}$

170 and $ATN_{extracted}$) were largely unchanged, loss of EC should be negligible. In the following

171 discussions, ΔATN, which is defined as $ATN_{extracted}–ATN_{untreated}$, will be introduced to quantify the

172 extraction-induced changes of ATN.

173   In the 2018–2019 campaign, ΔATN were close to zero for some of the samples, whereas for

174 the remaining ones, ATN typically decreased to varying degrees after the extraction (Figure 1a).

175 Here we noticed two distinct samples when exploring the ΔATN results (circled in Figure 1a). One

176 of them showed the most significant decrease of ATN after extraction (with a ΔATN of –0.32) during

177 the 2018–2019 measurement period, whereas ΔATN was also considerable for the other sample (–

178 0.25). The two distinct samples were collected successively during January 12–14, 2019. In this

179 period, relative humidity (RH) stayed above 85%, and both the sulfur oxidation ratio (SOR) and the

180 nitrogen oxidation ratio (NOR) exceeded 0.2, with record high concentrations of sulfate (~30 μg/m^3)

181 and nitrate (~40 μg/m^3) for the 2018–2019 winter. Given the enhanced production of secondary

182 inorganic aerosols, removal of nitrate by the extraction was a likely cause for the negative ΔATN of

183 the two distinct samples. Sulfate was not considered here, as it is insoluble in methanol. As another

184 component that could result in negative ΔATN, SOA could not be directly measured, whereas the

185 indirect estimating approaches such as the EC-tracer method typically required EC concentration.

186 We did not predict SOA at this stage, since the EC measurement uncertainties (e.g., the loss of EC

187 during extraction) had not been comprehensively evaluated. However, similar to SOA, formation of

188 sulfate and nitrate was contributed by both heterogeneous and gas-phase reactions (Liu et al., 2021;

189   Wang et al., 2023), indicating that it should be acceptable to reflect the production of secondary

190   aerosols (including SOA) based on a synthesis of SOR and NOR. In other words, it was very likely

191   that the atmospheric conditions with elevated SOR and NOR (e.g., January 12–14, 2019) were also

192   favorable for SOA formation (this inference would be validated in Section 3.3). For the two distinct

193   samples, therefore, the removal of scattering components, including not only nitrate but also SOA,

194   was inferred to be highly responsible for the considerable extraction-induced decreases of ATN.
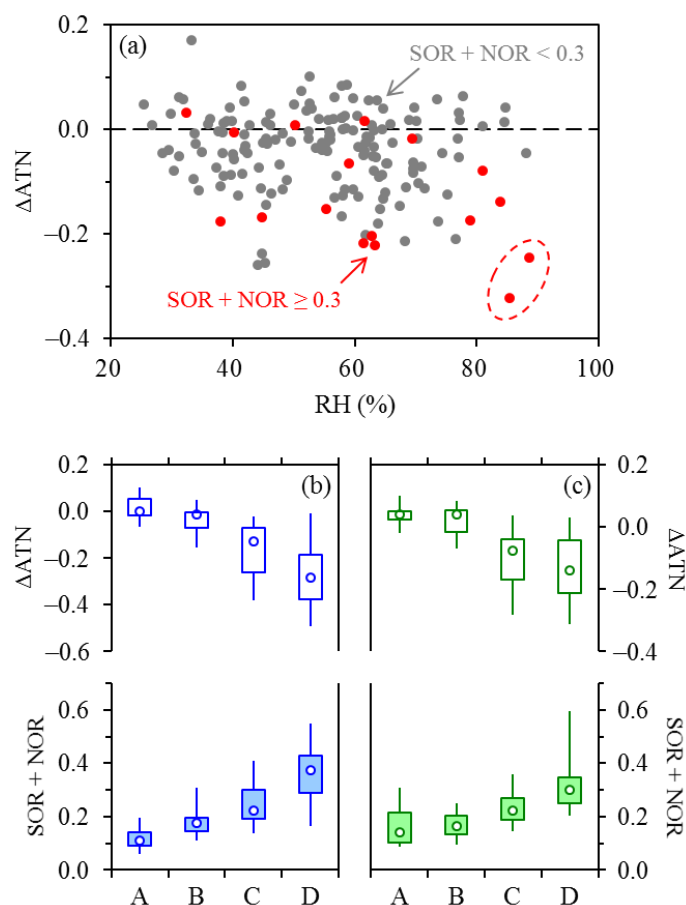
195

196   **Figure 1. (a)** Dependence of ΔATN, i.e., $ATN_{extracted}-ATN_{untreated}$, on RH during the 2018–2019
197   campaign, with results in different SOR + NOR ranges distinguished. The dashed line indicates a
198   ΔATN of zero. The dashed oval highlights two samples characterized by high RH levels, enhanced
199   formation of secondary aerosols, and considerable decreases of ATN after extraction. **(b)**

200 Comparisons of ΔATN (upper panel) and SOR + NOR (lower panel) across different RH ranges

201 (i.e., below 60%, 60–70%, 70–80% and above 80% as indicated by A–D, respectively) during the

202 2019–2020 campaign. To isolate the role of RH, only the samples with little influence of agricultural

203 fires were involved in the comparison. In each panel, lower and upper box bounds indicate the 25th

204 and 75th percentiles, the whiskers below and above the box indicate the 5th and 95th percentiles,

205 and the open circle within the box marks the median (the same hereinafter). **(c)** The same as (b) but

206 for 2021–2022.

207   Regarding the entire 2018–2019 campaign, humid events were actually uncommon, and most

208 samples with negative ΔATN values concentrated in the conditions with relatively low RH levels of

209 below 80 % (Figure 1a). Thus, in addition to the enhanced secondary aerosol production at high RH,

210 there must exist other influencing factors responsible for the change of ATN for the 2018–2019

211 samples. We then investigated the role of biomass burning, which could emit strongly-absorbing

212 BrC with mass absorption efficiencies comparable to black carbon (Alexander et al., 2008; Hoffer

213 et al., 2016; McClure et al., 2020). The 2018–2019 campaign was characterized by frequent

214 occurrences of agricultural fires (Figure S1), mainly in winter due to a one-off policy which crudely

215 approved a three-month long period (early December 2018 to early March 2019) for legitimate open

216 burning. In our previous studies (Cheng et al., 2021a), the fire episodes were identified by the

217 measured levoglucosan to organic carbon ratios (LG/OC*, where OC* indicates the untreated OC

218 based on IMPROVE-A) together with the satellite-based fire hotspots, and the 2018–2019 samples

219 were classified into three groups with increasing impacts of open burning. In this study, we revisited

220 the classifications using the levoglucosan to TC ratios (LG/TC), as the TC measurement was

221 independent of thermal-optical protocol. The classifications made by Cheng et al. (2021a) were

222 found to still hold, as LG/TC correlated strongly with LG/OC* ($r = 0.998$; Figure S2). As shown in

223 Figure 2a, ΔATN were close to zero under little impact of open burning. However, ΔATN turned

224 negative when the fire impacts were non-negligible, and the negative ΔATN values became more

225   considerable as the fire impacts increased. For the 2018–2019 campaign, therefore, the occurrences

226   of negative ΔATN were strongly associated with agricultural fires, e.g., through the removal of BrC

227   by extraction. In addition, both nitrate and NOR were found to increase with stronger influences of

228   agricultural fires (Figure S3), presumably due to the enhancement of nitrate production by open

229   burning emissions (Akagi et al., 2012; Collier et al., 2016; Liu et al., 2016b). Thus, although the

230   nitrate concentrations (Figure S3) were the lowest for 2018–2019 among the three campaigns, the

231   removal of nitrate by extraction could also be partially responsible for the association between

232   ΔATN and agricultural fires.

233
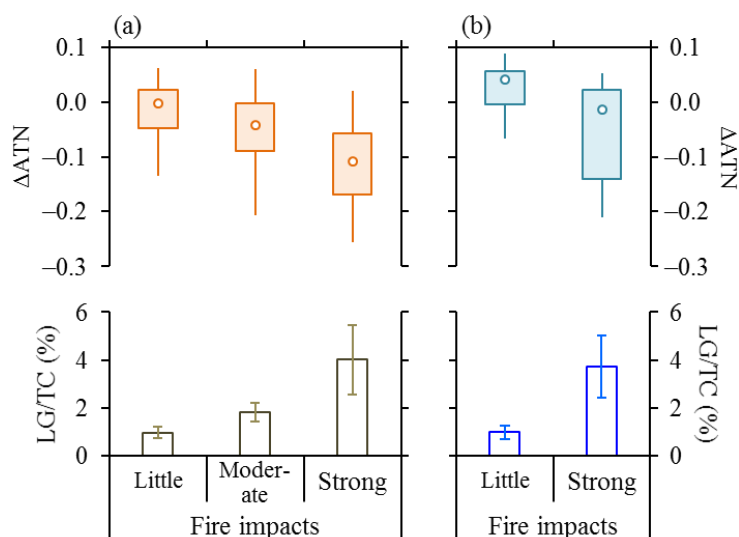
Figure 2. (a) Comparisons of ΔATN (upper panel) and LG/TC (on a basis of carbon mass; lower
panel) across three cases with increasing impacts of agricultural fires during the 2018–2019
campaign. To highlight the role of fires, the two distinct samples showing apparent influences of
RH (as circled in Figure 1a) were not involved in the comparisons. **(b)** Comparisons of ΔATN (upper
panel) and LG/TC (lower panel) between two cases with little and strong impacts of agricultural
fires during the 2020–2021 campaign. Only the samples with RH levels of below 70% were
involved, because (i) the influence of RH was insignificant for this RH range and (ii) the majority
of the 2020–2021 samples with strong fire impacts (24 out of 27) fell within this RH range. The
"moderate" case was not identified for 2020–2021. This is mainly because in response to different
policies on open burning, the agricultural fires spanned a relatively long period (more than two
months) during 2018–2019 but concentrated in April during 2020–2021 (Cheng et al., 2022).

245   Figures 1a and 2a suggest that ATN indeed decreased after the extraction for some of the 2018–

246   2019 samples. However, the negative ΔATN were found to be associated typically with agricultural

247   fires and occasionally with high RH conditions. The underlying mechanisms could be attributed

248   primarily to the removal of BrC and scattering components (including SOA and nitrate), respectively.

249   Importantly, ΔATN were negligible under little impact of agricultural fires (with a median value of

250   0.00; Figure 2a), suggesting that the loss of insoluble carbon (e.g., EC) should be negligible during

251   our extraction procedures.

252   In addition to the two distinct samples shown in Figure 1a, the connections between ΔATN and

253   RH could be further confirmed by the 2019–2020 campaign, which experienced much more high-

254   RH events (mainly in winter) compared to 2018–2019 (Figure S4). As shown in Figure 1b for the

255   2019–2020 samples with little impact of agricultural fires, the high-RH samples were characterized

256   by elevated SOR and NOR, pointing to enhanced formation of secondary aerosols (presumably

257   including SOA). A clear association was also observed between ΔATN and RH. ΔATN were

258   typically negligible when RH stayed below 70%, showing median ΔATN values of 0.00 and –0.01

259   for the RH ranges of below 60% and 60–70%, respectively. However, ΔATN deviated more

260   significantly from zero when RH further increased, e.g., with a median ΔATN value of –0.28 for the

261   RH range of above 80%. Although some primary organic compounds could also be non-absorbing

262   at 632 nm, it is unlikely that the abundances or emissions of such species would depend on RH.

263   Thus, the most possible explanation for the negative ΔATN observed at relatively high RH levels

264   should be the removal of secondary components (including SOA and nitrate) by extraction.

265   The 2019–2020 campaign covered a shorter period (Table 1) and encountered much fewer fire

266   episodes ($N = 2$) compared to 2018–2019 and 2019–2020 ($N = 21$ and 27, respectively). The two

13

267   2019–2020 samples with strong fire impacts had similar RH levels of ~50% and only one of them

268   exhibited considerable ΔATN (–0.26; Figure S5), which could be attributed to the removal of BrC

269   by extraction. For the 2019–2020 campaign, therefore, the extraction-induced decreases of ATN

270   were caused primarily by the removal of scattering components. In addition, as shown in Figure 1b,

271   the close-to-zero ΔATN values observed at the relatively low RH levels (e.g., with a median ΔATN

272   of 0.00 for the RH range of below 60%) further supported the inference on negligible loss of

273   insoluble carbon during extraction.

274   The 2020–2021 campaign experienced more high-RH events compared to 2018–2019 and

275   more agricultural-fire episodes than 2019–2020 (Figure S1). Correspondingly, the extraction-

276   induced changes of ATN could be attributed to the removal of either scattering components (Figure

277   1c) or BrC (Figure 2b). Similar to results from the other two campaigns, ΔATN were close to zero

278   for the 2020–2021 periods with low RH levels and little impact of open burning (Figure 1c),

279   demonstrating again that the extraction-induced loss of insoluble carbon was negligible.

280   The discussions above suggested that it was acceptable to attribute the reduced TC

281   concentrations in the extracted punches to the dissolving of organic compounds. This supported the

282   determination of MSOC as the difference in TC between the untreated and extracted punches, i.e.,

283    $TC_{untreated}$–$TC_{extracted}$. TC was used here since it was independent of analytical method, i.e., not

284   influenced by the uncertainties in the split of OC and EC. In addition, both $TC_{untreated}$ and $TC_{extracted}$

285   had been corrected by blanks before being used to calculate MSOC. A total of 53 filters were kept

286   as blanks for the three campaigns. They exhibited comparable TC loadings before and after the

287   extraction (averaging 0.61 ±0.23 and 0.44 ±0.21 $\mu gC/cm^3$, respectively), with no EC detected. This

288   also indicated that the methanol retained by the filters after the extraction could be completely

289   volatilized during the drying process, and consequently would not influence the split of OC and EC

290   for the extracted samples.

291   **3.2 Evaluation of EC from different methods**

292   As mentioned in Section 2.1, all the pairs of untreated and extracted punches were measured

293   by IMPROVE-A, with selected pairs also analyzed by NIOSH. A major purpose of involving

294   NIOSH was to unfold the EC discrepancies between different protocols, an important indicator for

295   the EC measurement uncertainties. The 2018–2019 campaign was characterized by intensive

296   agricultural fires in winter (Figure S1), providing an opportunity to evaluate the effects of open

297   burning emissions on EC determination. In addition, considering this campaign was the first one to

298   investigate EC measurement uncertainties in Northeast China, all the 2018–2019 samples were

299   analyzed by NIOSH (Table 1). The 2019–2020 campaign was characterized by unusually high levels

300   of RH in winter (Figure S1), which favored heterogeneous chemistry. To investigate the influences

301   of secondary aerosols on EC determination, NIOSH was applied to all the samples collected in

302   December 2019 and January 2020. The 2020–2021 campaign showed mixed features of the other

303   two campaigns, i.e., high RH events and agricultural fire episodes in January and April of 2021,

304   respectively (Figure S1). Thus all the samples from these two months were analyzed by NIOSH.

305   For the other periods of 2019–2020 and 2020–2021, NIOSH was used every five samples. As shown

306   in Table 1, a total of 339 pairs of untreated and extracted punches were analyzed by NIOSH in

307   addition to IMPROVE-A. Then for the majority of the Harbin samples (339 out of 486), there were

308   four sets of EC and OC results. Two sets were derived from the untreated punch, using the

309   IMPROVE-A and NIOSH protocols, respectively. For the third set, EC was measured by the

310   extracted punch based on IMPROVE-A ($EC_{extracted,\ IMPROVE-A}$) while OC was calculated as the

311 difference between $TC_{untreated}$ and $EC_{extracted, IMPROVE-A}$. OC and EC of the fourth set were defined

312 similarly based on NIOSH. The following patterns were observed when comparing the EC and OC

313 results across different methods.

314   First, only the OC to EC ratios determined by the untreated samples using IMPROVE-A, i.e.,

315 $(OC/EC)^*$, could properly reflect secondary aerosol formation. For a typical urban site,

316 anthropogenic emissions such as those from coal combustion and vehicles were usually considered

317 relatively stable during a given period, e.g., a specific season. Then the temporal variations of

318 OC/EC could be used to track SOA formation (e.g., as done by the EC-tracer method), after

319 excluding the episodes impacted by irregular emissions such as open burning and fireworks. As

320 firework events were not involved in this study, here we focused on three periods owing all the four

321 sets of OC and EC results with insignificant influence of agricultural fires, i.e., a four-week long

322 period in the 2018–2019 winter (December 28, 2018–January 25, 2019), December 2019 to January

323 2020, and January 2021. In the first case, three samples collected during January 12–15, 2019

324 exhibited persistently high levels of RH, SOR and NOR (Figure 3), pointing to enhanced formation

325 of secondary species possibly through heterogeneous chemistry. This humid period is supposed to

326 favor SOA production as well, since field observational results from the North China Plain

327 repeatedly showed concurrent increases of secondary inorganic and organic components under high

328 RH conditions in winter (Hu et al., 2016b; Liu et al., 2020; Sun et al., 2020). Similar to SOR and

329 NOR, $(OC/EC)^*$ also increased substantially for the humid period during January 12–15, 2019

330 (averaging 12.09 $\pm$0.97) compared to results from the other samples (averaging 5.39 $\pm$1.04; Figure

331 3). However, unlike $(OC/EC)^*$, OC to EC ratios determined in other approaches (namely OC/EC-I,

332 -II and -III) less accurately or failed to track the RH-dependent enhancement of SOA formation

333   (Figure S6). This conclusion also held for the other winters. Briefly, $(OC/EC)^*$ increased

334   concurrently with SOR and NOR at high RH levels for winters of both 2019–2020 (Figure 4) and

335   2020–2021 (Figure S7), whereas the alternative OC/EC ratios did not.

336
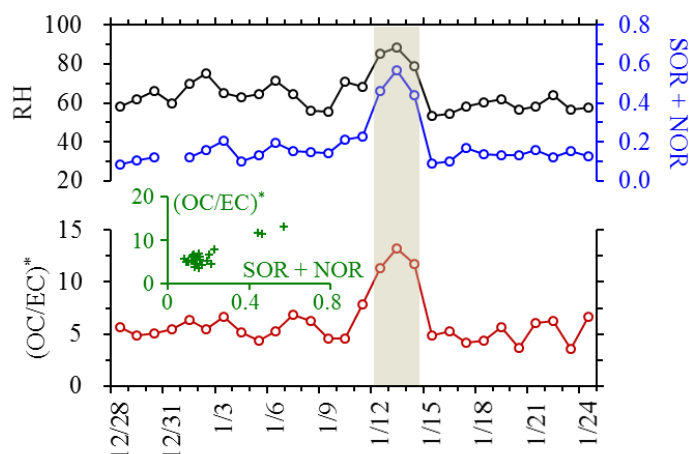
Figure 3. Temporal variations of RH, SOR +NOR (upper panel) and $(OC/EC)^*$ (lower panel) during
the 2018–2019 winter period with insignificant impact of agricultural fires. The shadowed area
highlights three distinct samples characterized by high RH and enhanced formation of secondary
aerosols. The inner scatter plot shows the positive dependence of $(OC/EC)^*$ on SOR + NOR ($r =$
0.89).

342
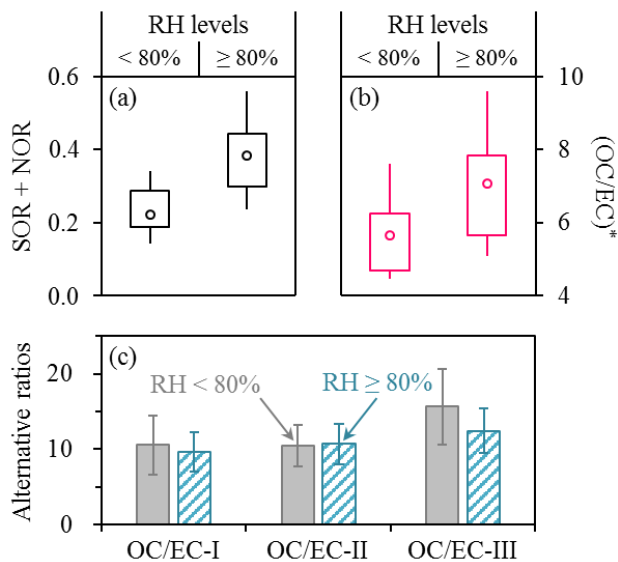
Figure 4. Comparisons of **(a)** SOR + NOR, **(b)** (OC/EC)* and **(c)** alternative OC/EC ratios between RH ranges of below and above 80%, based on results from December 2019–January 2020. In (c), OC/EC-I was derived from OC and EC measured by the untreated sample using NIOSH. OC/EC-II was calculated by $EC_{extracted, IMPROVE-A}$ and the corresponding OC (i.e., $TC_{untreated} - EC_{extracted, IMPROVE-A}$). OC/EC-III was determined similarly based on NIOSH.

Second, EC measured by the extracted filters ($EC_{extracted}$) were typically lower than results from the untreated ones ($EC_{untreated}$), especially for IMPROVE-A. This pattern should be attributed primarily to EC measurement uncertainties rather than EC loss during the extraction, as the later had been demonstrated to be negligible in Section 3.1. Two influencing factors were identified for the $EC_{extracted}$ to $EC_{untreated}$ ratios based on IMPROVE-A (defined as R_{IMPV}). The first one was the relative abundance of sulfate on the extracted filter, which could be estimated by the sulfate to $TC_{extracted}$ ratio (sulfate/$TC_{extracted}$). For the samples with little impact of open burning, R_{IMPV} tended to decrease as sulfate/$TC_{extracted}$ became higher, with generally consistent relationships for the three campaigns (Figure 5a). The median R_{IMPV} was 0.86 when the sulfate/$TC_{extracted}$ ratios were below 1, and decreased to 0.62 for the sulfate/$TC_{extracted}$ range of above 4 (Figure S8). We proposed the following hypotheses for the negative dependence of R_{IMPV} on sulfate/$TC_{extracted}$. We first simplified the remained particles on the extracted filters as a mixture of EC and sulfate, as nitrate and the vast majority of OC were soluble in methanol. Then a key assumption was that sulfate could promote the transmission of laser light through the extracted filters (e.g., by forward scattering; Petzold et al., 2005), indicating that the volatilization of sulfate during the inert mode of thermal-optical analysis could lead to a decrease of the transmittance signal (I). Thus in the oxidizing mode, a fraction of EC would be consumed to compensate this decrease (i.e. make I return to its initial value) and consequently, elemental carbon mass would be underestimated by $EC_{extracted}$.

In addition to sulfate/$TC_{extracted}$, another influencing factor for R_{IMPV} was open burning. R_{IMPV}

367   determined for the agricultural-fire episodes were lower compared to results from the periods with

368   the same sulfate/$TC_{extracted}$ range but little impact of open burning (Figures 5b and 5c). As discussed

369   in Section 3.1, agricultural fires could be a source for strongly-absorbing BrC. For the untreated

370   filters, such BrC could be difficult to be properly distinguished from EC by the carbon analyzer used

371   in this study. Thus, a possible explanation for the reduced R_{IMPV} under strong impacts of agricultural

372   fires was that open burning emissions could result in overestimation of elemental carbon mass by

373    $EC_{untreated}$ (i.e., the positive artifact). Under this assumption, the fire-induced decreases of R_{IMPV}

374   could be translated into positive artifacts of ~25% (based on the median R_{IMPV} determined under

375   little and strong fire impacts) for the open burning episodes of 2018–2019 and 2020–2021.

376
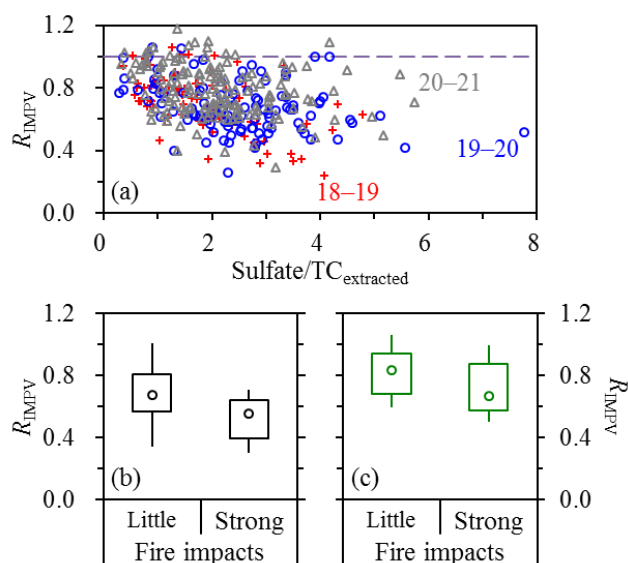
Figure 5. (a) Dependence of R_{IMPV} (i.e., the $EC_{extracted}$ to $EC_{untreated}$ ratio based on IMPROVE-A) on
sulfate/$TC_{extracted}$, with results from different campaigns shown separately. Only the samples with
little influence of open burning were involved. **(b)** Comparison of R_{IMPV} between the 2018–2019
samples with strong impacts of agricultural fires (as indicated by "Strong") and those with the same
sulfate/$TC_{extracted}$ range but little fire impact (as indicated by "Little"). **(c)** The same as (b) but for
2020–2021.

383   Similar to R_{IMPV}, the $EC_{extracted}$ to $EC_{untreated}$ ratios based on NIOSH (R_{NOSH}) also tended to

19

384 decrease with increasing sulfate/$TC_{extracted}$, e.g., with the median R_{NOSH} decreasing from 1.00 to 0.78

385 as sulfate/$TC_{extracted}$ became higher (Figure S8). Thus, the inference on the underestimation of

386 elemental carbon mass by $EC_{extracted}$ should be valid for NIOSH as well. The close-to-one R_{NIOSH}

387 but lower $R_{IMPROVE-A}$ (0.86) determined for the same sulfate/$TC_{extracted}$ range of below 1 (Figure S8)

388 suggested that the extraction led to comparable $EC_{untreated}$ and $EC_{extracted}$ when using NIOSH but

389 resulted in relatively low $EC_{extracted}$ when using IMPROVE-A. This prohibited the use of $EC_{untreated}$

390 vs. $EC_{extracted}$ relationship for the assessment of EC loss during extraction, and highlighted the

391 significance of the ΔATN-based evaluation results in Section 3.1. It is also noteworthy that a

392 considerable number of samples showed R_{NIOSH} values above 1, indicating that $EC_{untreated}$ was even

393 lower than $EC_{extracted}$ when analyzing these samples by NIOSH. A possible explanation was that the

394 NIOSH-based $EC_{untreated}$ also underestimated the elemental carbon mass, i.e., both $EC_{extracted}$ and

395 $EC_{untreated}$ were biased low (more significantly for the latter) when applying NIOSH to the Harbin

396 samples. In addition, no evidence was observed for apparent influence of open burning on R_{NIOSH}

397 (Figure S9). It appeared that the determination of $EC_{untreated}$ was less significantly affected by

398 agricultural fires when using NIOSH compared to IMROVE-A.

399 The third pattern derived from the comparison of EC results across different methods was that

400 for the untreated samples, the IMRPROVE-A protocol led to higher EC values than NIOSH (Figure

401 6). This pattern was in line with results from other regions (e.g., Chow et al., 2004; Piazzalunga et

402 al., 2011; Giannoni et al., 2016), and was consistent with the previous inference on the uncertainty

403 of the NIOSH-based $EC_{untreated}$. In addition, the discrepancies between $EC_{untreated}$ measured by the

404 two protocols became larger with increasing impacts of agricultural fires (Figure 6). This trend could

405 be attributed to the open-burning-induced overestimation of elemental carbon mass by $EC_{untreated}$

406 (i.e., the positive artifact), which was considerable for IMPROVE-A (Figures 5b and 5c) but

407 appeared insignificant when using NIOSH (Figure S9). Another noteworthy feature in Figure 6 was

408 that compared to the open burning episodes of 2020–2021, the 2018–2019 fire events showed more

409 significant inter-protocol differences in $EC_{untreated}$. The contrast appeared to indicate that the 2018–

410 2019 fires, which were inferred to have lower combustion efficiencies (Cheng et al., 2022), could

411 result in more significant positive artifacts for IMPROVE-A.

412
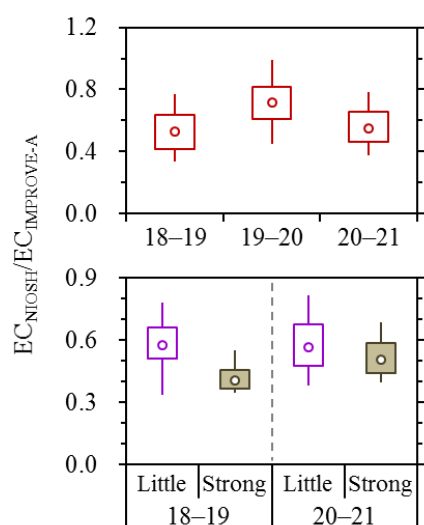
Figure 6. Ratios between EC measured by different protocols using the untreated samples, i.e.,
$EC_{NIOSH}/EC_{IMPROVE-A}$. The upper panel compares the ratios across campaigns. The lower panel
compares the ratios between the samples with little and strong impacts of agricultural fires, with
results from 2018–2019 and 2020–2021 shown separately.

417 As reflected by the discussions above, all the EC results had uncertainties, regardless of the

418 pretreatment approaches (with or without methanol extraction) and temperature protocols

419 (IMPROVE-A or NIOSH). For the untreated samples, the IMRPOVE-A protocol led to OC/EC

420 ratios in reasonable accordance with secondary aerosol formation, whereas NIOSH did not.

421 However, it must be acknowledged that for IMPROVE-A, the elemental carbon mass was likely

422   overestimated by EC$_{untreated}$ under strong impacts of agricultural fires (by ~25%), presumably due to

423   the interference of BrC. Although this positive artifact could in principle be reduced or minimized

424   by methanol extraction, a new issue arose that the elemental carbon mass was underestimated by

425   EC$_{extracted}$ (i.e., the negative artifact), which was inferred to be associated with the volatilization of

426   sulfate from the extracted samples during the inert mode of thermal-optical analysis. The

427   significance of the negative artifact could be reflected by decreases of EC after extraction, which

428   were as high as ~15–40% for IMPROVE-A (Figure S8). Importantly, the negative artifact was not

429   limited to the open-burning-impacted samples, i.e., it also biased the measurement of samples with

430   little influence of agricultural fires. Thus, although the methanol extraction could reduce the positive

431   artifacts of EC$_{untreated}$ for the fire episodes, it in turn caused more significant negative artifacts of

432   EC$_{extracted}$ for all the Harbin samples. Consequently, the methanol extraction was not considered an

433   effective approach to improve the measurement of elemental carbon mass in this study. In the

434   following discussions, the EC$_{untreated}$ results based on IMPROVE-A, i.e., EC*, will be used for

435   exploring the sources of light-absorbing carbon in Harbin.

3.3 Sources of light-absorbing carbon

437   Based on the observational results, EPA's Positive Matrix Factorization (PMF) model (version

438   5.0) was used to elucidate the sources of light-absorbing carbonaceous aerosols. Here we focus on

439   the 2020–2021 campaign, which experienced coexisted features of 2018–2019 and 2019–2020 (i.e.,

440   strong impacts of agricultural fires and high-RH conditions, respectively). A six-factor solution was

441   resolved by PMF (Figure S10), using time series of EC*, BrC mass concentration (i.e., MSOC),

442   light absorption coefficient of BrC at 365 nm [i.e., $(b_{abs})_{365}$], levoglucosan, chloride, sulfate, nitrate

443   and ammonium as inputs. Briefly, two factors were considered secondary due to their dominant

444   contributions to secondary inorganic ions; two factors were attributed to primary emissions from

445   biomass burning (BB), as they explained the vast majority of levoglucosan; the last two factors were

446   important contributors to EC and chloride but had little levoglucosan or secondary species, pointing

447   to primary emissions from non-BB sources (e.g., coal combustion and vehicles). MSOC apportioned

448   into these three source categories were termed as sec-MSOC, pri-MSOC$_{BB}$ and pri-MSOC$_{non-BB}$,

449   respectively. Source-resolved BrC light absorption were defined similarly, as sec-BrC, pri-BrC$_{BB}$

450   and pri-BrC$_{non-BB}$. EC* emitted by the BB and non-BB sources were referred to as EC$_{BB}$ and EC$_{non-BB}$,

451   respectively. Figure 7 presents an overview of the source apportionment results. The temporal

452   variations of the MSOC and $(b_{abs})_{365}$ source attributions were characterized by considerable

453   increases of the BB contribution in April, the season with frequent occurrences of agricultural fires.

454   It was also noticed that secondary formation was an important source of MSOC (especially in winter)

455   but contributed less significantly to $(b_{abs})_{365}$. This pattern could be attributed to the fact that

456   secondary BrC was typically less absorbing than primary BrC (Kumar et al., 2018; Cappa et al.,

457   2020). For the sources of EC*, a noteworthy feature was that the BB contributions reached similarly

458   higher levels in the fire-impacted April and January, the coldest month with little influence of open

459   burning.

460   The revised CMAQ predicted the concentrations of organic and elemental carbon (i.e., OC$_{mod}$

461   and EC$_{mod}$), with the primary and secondary OC (i.e., POC$_{mod}$ and SOC$_{mod}$) results also available.

462   Given that MSOC approximately equaled OC* (Figure S11), it should be acceptable to perform

463   direct comparisons between these two terms from various sources, i.e., between SOC$_{mod}$ and sec-

464   MSOC, and between POC$_{mod}$ and primary MSOC (pri-MSOC, calculated as the sum of pri-MSOC$_{BB}$

465   and pri-MSOC$_{non-BB}$). For the samples with little influence of agricultural fires, the revised CMAQ

466   generally reproduced the observation-based pri-MSOC and EC* (Figure 8a), with mean biases of –

467   1.94 μgC/m³ and −0.43 μgC/m³, respectively. In this case, the POC_{mod} to EC_{mod} ratios also coincided

468   with the measurement results, i.e., the pri-MSOC to EC* ratios. For example, the two ratios agreed

469   with respect to both the absolute values and seasonal variations (Figure 8b). These consistencies to

470   some extent supported the reliability of the source apportionment results from PMF.
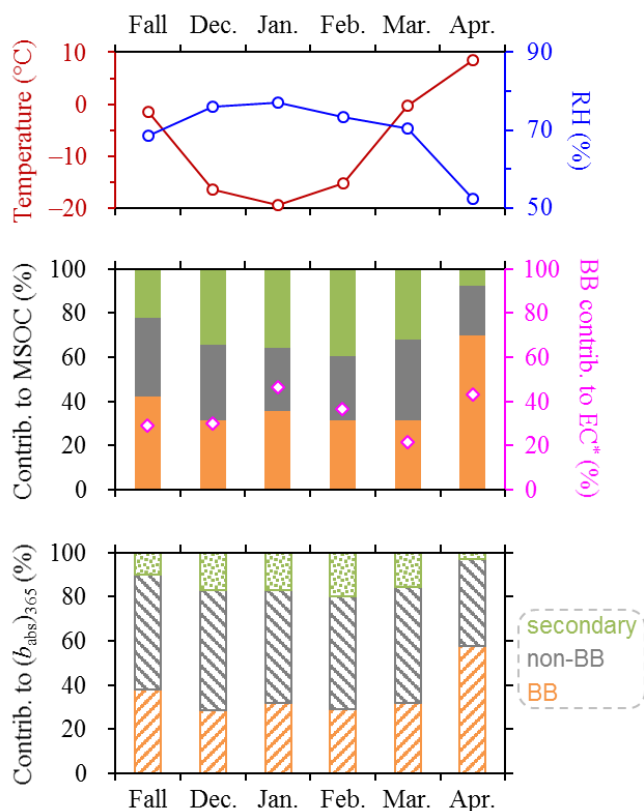
471

472   **Figure 7.** Monthly-averaged temperatures and RH (upper panel), and source apportionment results
473   of MSOC, EC (middle panel) and $(b_{abs})_{365}$ (lower panel) for the 2020–2021 campaign. Fall indicates
474   mid-October to November. In the middle and lower panels, sources of MSOC and $(b_{abs})_{365}$ were
475   classified into three categories distinguished by different colors in the bar charts, i.e., primary BB
476   emissions in orange, primary non-BB emissions in grey and secondary in green. Sources of EC*
477   were separated into BB and non-BB emissions, with the BB contributions shown by the diamonds
478   in the middle panel.
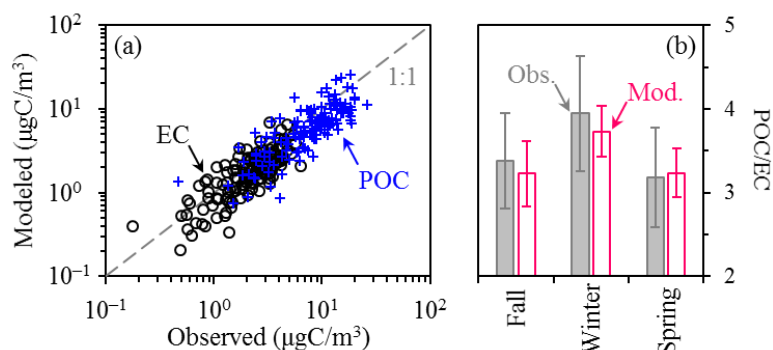
Figure 8. Comparisons of the modeled and observed **(a)** POC and EC concentrations, and **(b)** the seasonal POC to EC ratios for the 2020–2021 campaign. Only the samples with little fire impact were involved. The 1:1 line is also shown in (a).

The high-RH conditions were concentrated in the winter, i.e., December 2020 to February 2021. Such conditions were believed to favor SOA production, as indicated by the RH-dependent increases of SOR and NOR (Figures 1b and 1c). This inference was further confirmed by the PMF results, as both the sec-MSOC and sec-MSOC/EC* were considerably enhanced after RH exceeding 80% (Figure 9). The PMF results also confirmed the link between (OC/EC)* and SOA formation, given the agreement between sec-MSOC and results from the EC-tracer method ($r = 0.91$; Figure S12). The revised CMAQ predicted the RH-dependent enhancement of SOC formation as well. However, it failed to reproduce the observed SOC concentrations and SOC to EC ratios, with significant underestimations. For example, the modeling results only explained 18% and 22% of the observed SOC concentrations (corresponding to 19% and 26% of the observed SOC to EC ratios) for the RH ranges of below and above 80%, respectively. The results suggested that the SOA module of the revised CMAQ, including the newly-added heterogeneous mechanisms, still required substantial improvements.
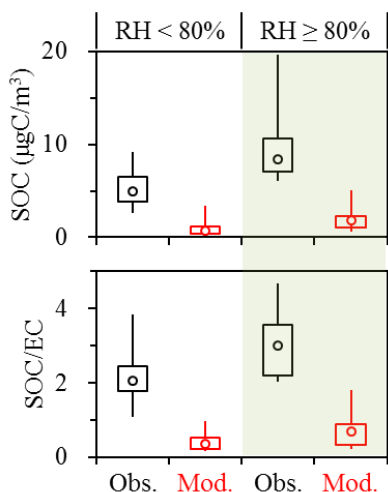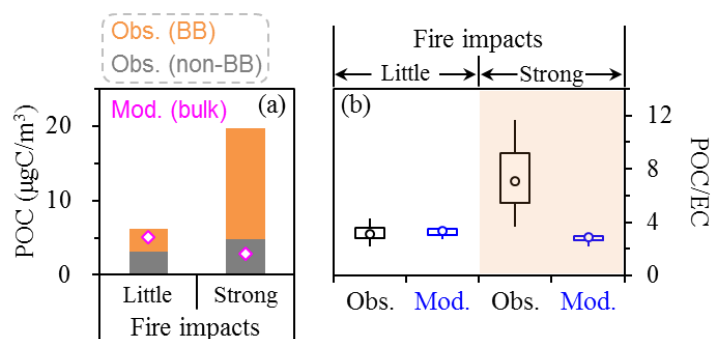
Figure 9. Comparisons of the modeled and observed SOC concentrations (upper panel) and SOC to EC ratios (lower panel) for the 2020–2021 winter. The comparisons were performed for the RH ranges of below and above 80% separately. Open burning impact was negligible for this period.

The agricultural fire episodes mainly occurred in April during the 2020–2021 measurement period. PMF results suggested that the BB contributions to MSOC and EC* increased significantly for the fire episodes (reaching 72 and 44%, respectively) compared to other periods in spring (33 and 25%, respectively). The fire emissions also significantly increased the observation-based POC concentrations (i.e., pri-MSOC) and POC to EC ratios (i.e., pri-MSOC/EC*; Figure 10). This is within expectation, since organic compounds were frequently found to constitute the vast majority of the particulate emissions from open burning emissions (Hodgson et al., 2018; Garofalo et al., 2019). Since the revised CMAQ did not predict biomass burning OC separately, comparison of the modeling and observational results could only be made based on the bulk primary OC. As shown in Figure 10, the model could not track the influences of agricultural fires on primary OC, e.g., as indicated by the largely comparable POC_{mod} to EC_{mod} ratios between the fire episodes and other periods in spring. It appeared that the fire emissions, which were derived from the FINN inventory, were underestimated for the model simulation. In FINN, the open burning emissions were retrieved

513   using burned areas detected by the Terra and Aqua polar-orbiting satellites (Wiedinmyer et al., 2011).

514   A limitation of this approach was the missing of fires due to satellite overpass timing (Uranishi et

515   al., 2019), which was also the case for the Global Fire Emissions Database (GFED), another

516   commonly-used open burning inventory based on burned areas (Konovalov et al., 2018; Chen et al.,

517   2023). Previous studies suggested that the underestimation of open burning emissions by FINN or

518   GFED could be considerable, e.g., by a factor of as high as above 20 (Xie et al., 2024). Given the

519   massive agricultural sector in Harbin and surrounding areas (e.g., the Harbin-Changchun

520   metropolitan area), we suggest that the uncertainties of open burning inventories merit particular

521   attention for the modeling studies in this region.

522

Figure 10. Comparisons of the modeled and observed **(a)** POC concentrations and **(b)** POC to EC
ratios between the samples with little and strong fire impacts in the spring of 2021. In (a), the
observation-based results were shown by the bars (as the sum of BB and non-BB emissions), while
the modeling results were indicated by the diamonds.

527   **4. Conclusions and atmospheric implications**

528   Light-absorbing carbonaceous aerosols were investigated for Northeast China based on three

529   campaigns conducted during 2018–2021 in Harbin. BrC masses were determined based on methanol

530   extraction of filter samples, as the difference between TC concentrations of the untreated and

531   extracted punches. A long-standing concern on this method was the loss of EC during extraction.

532   This artifact was evaluated indirectly based on the extraction-induced changes of ATN, due to the

533   lack of reference method for EC measurement. For different campaigns, it was repeatedly observed

534   that ATN was largely unchanged after extraction, as long as the RH levels were unfavorable for

535   secondary aerosol formation and the impacts of agricultural fires were negligible. This pointed to

536   negligible loss of EC during extraction and consequently supported the robustness of the

537   observational data on BrC mass. In addition, EC and OC concentrations were determined by four

538   methods differing with respect to pretreatment approaches (with and without extraction of the filter

539   samples) and thermal-optical protocols (IMPROVE-A and NIOSH). Results from the untreated

540   samples using IMPROVE-A were found to provide OC to EC ratios in reasonable accordance with

541   secondary aerosol formation. Thus EC determined by this method was used for the source

542   apportionment of light-absorbing carbon, together with other input species such as BrC mass, BrC

543   absorption coefficient and levoglucosan.

544   The observation-based source apportionment results showed increased contributions of

545   secondary formation to BrC in winter, when the high-RH conditions concentrated. It was also

546   noticed that secondary formation contributed more significantly to BrC mass than BrC absorption,

547   in line with the consensus that secondary BrC was typically less absorbing than primary BrC. In

548   addition, agricultural fires were found to effectively enhance the BB contributions to BrC (in terms

549   of either mass concentration or absorption coefficient) and EC.

550   The abundances and sources of OC and EC were also predicted by an air quality model with

551   newly-added heterogeneous reactions. The general equivalence of BrC and OC masses supported

552   direct comparisons of the observational and modeling results. The model properly reproduced POC

553   and EC (in terms of both absolute concentration and POC to EC ratio) for the periods with little

554   impact of agricultural fires. The model also predicted the existence of RH-dependent enhancement

555   of SOC production in winter, but significantly underestimated the observed SOC concentrations.

556   Another problem identified for the modeling results was the substantial underprediction of POC for

557   the agricultural fire events, presumably due to underestimation of open burning emissions by the

558   FINN inventory.

559   An agreement between observed and simulated results (e.g., with respect to aerosol abundances

560   and sources) is essential for the development of efficient air pollution control strategies. In this study,

561   we constrained the modeling results of carbonaceous aerosols by field observation, based on

562   validated measurement results of BrC and EC. Two challenges were identified for the simulation of

563   carbonaceous aerosols in Northeast China, i.e., significant underprediction of SOC and agricultural

564   fire emissions. Our results suggest that the commonly-used CMAQ model requires substantial

565   improvements for the application in Northeast China.

566   **Data availability.** Data are available from the corresponding author upon request

567   (jiumengliu@hit.edu.cn).

568   **Author contributions.** YC and JL designed the study and prepared the paper, with inputs from all

569   the co-authors. XC and ZZ carried out the experiments. SZ and HZ performed the simulations. QZ

570   and KH validated the results and supervised the study.

571   **Competing interests.** At least one of the (co-)authors is a member of the editorial board of

572   Atmospheric Chemistry and Physics.

573   **Disclaimer.** Publisher's note: Copernicus Publications remains neutral with regard to jurisdictional

574   claims in published maps and institutional affiliations.

575   **Acknowledgements.** The authors thank Zhen-yu Du at the National Research Center for

576 Environmental Analysis and Measurement and Lin-lin Liang at the Chinese Academy of

577 Meteorological Sciences for their help in sample analysis.

580 **References**

581 Akagi, S. K., Craven, J. S., Taylor, J. W., McMeeking, G. R., Yokelson, R. J., Burling, I. R., Urbanski,
582   S. P., Wold, C. E., Seinfeld, J. H., Coe, H., Alvarado, M. J., and Weise, D. R.: Evolution of
583   trace gases and particles emitted by a chaparral fire in California, *Atmos. Chem. Phys.*, 12,
584   1397–1421, https://doi.org/10.5194/acp-12-1397-2012, 2012.

585 Alexander, D. T. L., Crozier, P. A., and Anderson, J. R.: Brown carbon spheres in East Asian outflow
586   and their optical properties, *Science*, 321, 833–836, https://doi.org/10.1126/science.1155296,
587   2008.

588 Baumgardner, D., Popovicheva, O., Allan, J., Bernardoni, V., Cao, J., Cavalli, F., Cozic, J., Diapouli,
589   E., Eleftheriadis, K., Genberg, P. J., Gonzalez, C., Gysel, M., John, A., Kirchstetter, T. W.,
590   Kuhlbusch, T. A. J., Laborde, M., Lack, D., Müller, T., Niessner, R., Petzold, A., Piazzalunga,
591   A., Putaud, J. P., Schwarz, J., Sheridan, P., Subramanian, R., Swietlicki, E., Valli, G., Vecchi,
592   R., and Viana, M.: Soot reference materials for instrument calibration and intercomparisons: a
593   workshop summary with recommendations, *Atmos. Meas. Tech.*, 5, 1869–1887,
594   https://doi.org/10.5194/amt-5-1869-2012, 2012.

595 Bond, T. C., Doherty, S. J., Fahey, D. W., Forster, P. M., Berntsen, T., DeAngelo, B. J., Flanner, M.
596   G., Ghan, S., Kärcher, B., Koch, D., Kinne, S., Kondo, Y., Quinn, P. K., Sarofim, M. C., Schultz,
597   M. G., Schulz, M., Venkataraman, C., Zhang, H., Zhang, S., Bellouin, N., Guttikunda, S. K.,
598   Hopke, P. K., Jacobson, M. Z., Kaiser, J. W., Klimont, Z., Lohmann, U., Schwarz, J. P., Shindell,
599   D., Storelvmo, T., Warren, S. G., and Zender, C. S.: Bounding the role of black carbon in the
600   climate system: a scientific assessment, *J. Geophys. Res.*, 118, 5380–5552,
601   https://doi.org/10.1002/jgrd.50171, 2013.

602 Buffaloe, G. M., Lack, D. A., Williams, E. J., Coffman, D., Hayden, K. L., Lerner, B. M., Li, S. M.,
603   Nuaaman, I., Massoli, P., Onasch, T. B., Quinn, P. K., and Cappa, C. D.: Black carbon
604   emissions from in-use ships: a California regional assessment, *Atmos. Chem. Phys.*, 14, 1881–
605   1896, https://doi.org/10.5194/acp-14-1881-2014, 2014.

606 Cappa, C. D., Lim, C. Y., Hagan, D. H., Coggon, M., Koss, A., Sekimoto, K., de Gouw, J., Onasch,
607   T. B., Warneke, C., and Kroll, J. H.: Biomass-burning-derived particles from a wide variety of
608   fuels – Part 2: effects of photochemical aging on particle optical and chemical properties,
609   *Atmos. Chem. Phys.*, 20, 8511–8532, https://doi.org/10.5194/acp-20-8511-2020, 2020.

610 Cavalli, F., Viana, M., Yttri, K. E., Genberg, J., and Putaud, J. P.: Toward a standardized thermal-
611   optical protocol for measuring atmospheric organic and elemental carbon: the EUSAAR

612   protocol, ***Atmos. Meas. Tech.***, 3, 79–89, https://doi.org/10.5194/amt-3-79-2010, 2010.

613 Chen, K. P., Raeofy, N., Lum, M., Mayorga, R., Woods, M., Bahreini, R., Zhang, H. F., and Lin, Y.
614   H.: Solvent effects on chemical composition and optical properties of extracted secondary
615   brown carbon constituents, ***Aerosol Sci. Technol.***, 56, 917–930,
616   https://doi.org/10.1080/02786826.2022.2100734, 2022.

617 Chen, L. J., Gao, Y., Ma, M. C., Wang, L. L., Wang, Q. L., Guan, S. H., Yao, X. H., and Gao, H. W.:
618   Striking impacts of biomass burning on $PM_{2.5}$ concentrations in Northeast China through the
619   emission inventory improvement, ***Environ. Pollut.***, 318, 120835,
620   https://doi.org/10.1016/j.envpol.2022.120835, 2023.

621 Chen, Q., Ikemori, F., Nakamura, Y., Vodicka, P., Kawamura, K., and Mochida, M.: Structural and
622   light-absorption characteristics of complex water-insoluble organic mixtures in urban
623   submicrometer aerosols, ***Environ. Sci. Technol.***, 51, 8293–8303,
624   https://doi.org/10.1021/acs.est.7b01630, 2017.

625 Chen, Y., and Bond, T. C.: Light absorption by organic carbon from wood combustion, ***Atmos.***
626   ***Chem. Phys.***, 10, 1773–1787, https://doi.org/10.5194/acp-10-1773-2010, 2010.

627 Cheng, Y., Cao, X. B., Liu, J. M., Yu, Q. Q., Zhong, Y. J., Geng, G. N., Zhang, Q., and He, K. B.:
628   New open burning policy reshaped the aerosol characteristics of agricultural fire episodes in
629   Northeast China, ***Sci. Total. Environ.***, 810, 52272,
630   https://doi.org/10.1016/j.scitotenv.2021.152272, 2022.

631 Cheng, Y., Yu, Q., Liu, J., Cao, X., Zhong, Y., Du, Z., Liang, L., Geng, G., Ma, W., Qi, H., Zhang,
632   Q., and He, K.: Dramatic changes in Harbin aerosol during 2018–2020: the roles of open
633   burning policy and secondary aerosol formation, ***Atmos. Chem. Phys.***, 21, 15199–15211,
634   https://doi.org/10.5194/acp-21-15199-2021, 2021a.

635 Cheng, Z. Z., Atwi, K., El Hajj, O., Ijeli, I., Al Fischer, D., Smith, G., and Saleh, R.: Discrepancies
636   between brown carbon light-absorption properties retrieved from online and offline
637   measurements, ***Aerosol Sci. Technol.***, 55, 92–103,
638   https://doi.org/10.1080/02786826.2020.1820940, 2021b.

639 Chow, J. C., Watson, J. G., Chen, L. W. A., Arnott, W. P., and Moosmüller, H.: Equivalence of
640   elemental carbon by thermal/optical reflectance and transmittance with different temperature
641   protocols, ***Environ. Sci. Technol.***, 38, 4414–4422, https://doi.org/10.1021/es034936u, 2004.

642 Chow, J. C., Watson, J. G., Chen, L. W. A., Chang, M. O., Robinson, N. F., Trimble, D., and Kohl,
643   S.: The IMPROVE-A temperature protocol for thermal/optical carbon analysis: maintaining
644   consistency with a long-term database, ***J. Air Waste Manage. Assoc.***, 57, 1014–1023,
645   https://doi.org/10.3155/1047-3289.57.9.1014, 2007.

646 Collier, S., Zhou, S., Onasch, T. B., Jaffe, D. A., Kleinman, L., Sedlacek, A. J., Briggs, N. L., Hee,
647   J., Fortner, E., Shilling, J. E., Worsnop, D., Yokelson, R. J., Parworth, C., Ge, X. L., Xu, J. Z.,
648   Butterfield, Z., Chand, D., Dubey, M. K., Pekour, M. S., Springston, S., and Zhang, Q.:
649   Regional influence of aerosol emissions from wildfires driven by combustion efficiency:
650   insights from the BBOP campaign, ***Environ. Sci. Technol.***, 50, 8613–8622,

651   https://doi.org/10.1021/acs.est.6b01617, 2016.

652   Corbin, J. C., Czech, H., Massabò, D., de Mongeot, F. B., Jakobi, G., Liu, F., Lobo, P., Mennucci,
653   C., Mensah, A. A., Orasche, J., Pieber, S. M., Prévôt, A. S. H., Stengel, B., Tay, L. L., Zanatta,
654   M., Zimmermann, R., El Haddad, I., and Gysel, M.: Infrared-absorbing carbonaceous tar can
655   dominate light absorption by marine-engine exhaust, *npj Clim. Atmos. Sci.*, 2, 12,
656   https://doi.org/10.1038/s41612-019-0069-5, 2019.

657   Gao, C. Y., Heald, C. L., Katich, J. M., Luo, G., and Yu, F. Q.: Remote aerosol simulated during the
658   Atmospheric Tomography (ATom) campaign and implications for aerosol lifetime, *J. Geophys.*
659   *Res. Atmos.*, 127, e2022JD036524, https://doi.org/10.1029/2022JD036524, 2022.

660   Garofalo, L. A., Pothier, M. A., Levin, E. J. T., Campos, T., Kreidenweis, S. M., and Farmer, D. K.:
661   Emission and evolution of submicron organic aerosol in smoke from wildfires in the Western
662   United   States,   *ACS   Earth   Space   Chem.*,   3,   1237–1247,
663   https://doi.org/10.1021/acsearthspacechem.9b00125, 2019.

664   Giannoni, M., Calzolai, G., Chiari, M., Cincinelli, A., Lucarelli, F., Martellini, T., and Nava, S.: A
665   comparison between thermal-optical transmittance elemental carbon measured by different
666   protocols   in   PM$_{2.5}$ samples,   *Sci.   Total   Environ.*,   571,   195–205,
667   https://doi.org/10.1016/j.scitotenv.2016.07.128, 2016.

668   Hecobian, A., Zhang, X., Zheng, M., Frank, N., Edgerton, E. S., and Weber, R. J.: Water-soluble
669   organic aerosol material and the light-absorption characteristics of aqueous extracts measured
670   over   the   Southeastern   United   States,   *Atmos.   Chem.   Phys.*,   10,   5965–5977,
671   https://doi.org/10.5194/acp-10-5965-2010, 2010.

672   Hodgson, A. K., Morgan, W. T., O'Shea, S., Bauguitte, S., Allan, J. D., Darbyshire, E., Flynn, M. J.,
673   Liu, D., Lee, J., Johnson, B., Haywood, J. M., Longo, K. M., Artaxo, P. E., and Coe, H.: Near-
674   field emission profiling of tropical forest and Cerrado fires in Brazil during SAMBBA 2012,
675   *Atmos. Chem. Phys.*, 18, 5619–5638, https://doi.org/10.5194/acp-18-5619-2018, 2018.

676   Hoffer, A., Tóth, A., Nyirő-Kósa, I., Pósfai, M., and Gelencsér, A.: Light absorption properties of
677   laboratory-generated   tar   ball   particles,   *Atmos.   Chem.   Phys.*,   16,   239–246,
678   https://doi.org/10.5194/acp-16-239-2016, 2016.

679   Hu, J. L., Chen, J. J., Ying, Q., and Zhang, H. L.: One-year simulation of ozone and particulate
680   matter in China using WRF/CMAQ modeling system, Atmos. Chem. Phys., 16, 10333–10350,
681   https://doi.org/10.5194/acp-16-10333-2016, 2016a.

682   Hu, W. W., Hu, M., Hu, W., Jimenez, J. L., Yuan, B., Chen, W. T., Wang, M., Wu, Y. S., Chen, C.,
683   Wang, Z. B., Peng, J. F., Zeng, L. M., and Shao, M.: Chemical composition, sources, and aging
684   process of submicron aerosols in Beijing: contrast between summer and winter, *J. Geophys.*
685   *Res. Atmos.*, 121, 1955–1977, https://doi.org/10.1002/2015JD024020, 2016b.

686   Koch, D., Schulz, M., Kinne, S., McNaughton, C., Spackman, J. R., Balkanski, Y., Bauer, S.,
687   Berntsen, T., Bond, T. C., Boucher, O., Chin, M., Clarke, A., De Luca, N., Dentener, F., Diehl,
688   T., Dubovik, O., Easter, R., Fahey, D. W., Feichter, J., Fillmore, D., Freitag, S., Ghan, S.,
689   Ginoux, P., Gong, S., Horowitz, L., Iversen, T., Kirkevåg, A., Klimont, Z., Kondo, Y., Krol,

690   M., Liu, X., Miller, R., Montanaro, V., Moteki, N., Myhre, G., Penner, J. E., Perlwitz, J., Pitari,
691   G., Reddy, S., Sahu, L., Sakamoto, H., Schuster, G., Schwarz, J. P., Seland, Ø., Stier, P.,
692   Takegawa, N., Takemura, T., Textor, C., van Aardenne, J. A., and Zhao, Y.: Evaluation of black
693   carbon estimations in global aerosol models, *Atmos. Chem. Phys.*, 9, 9001–9026,
694   https://doi.org/10.5194/acp-9-9001-2009, 2009.

695   Konovalov, I. B., Lvova, D. A., Beekmann, M., Jethva, H., Mikhailov, E. F., Paris, J.-D., Belan, B.
696   D., Kozlov, V. S., Ciais, P., and Andreae, M. O.: Estimation of black carbon emissions from
697   Siberian fires using satellite observations of absorption and extinction optical depths, *Atmos.*
698   *Chem. Phys.*, 18, 14889–14924, https://doi.org/10.5194/acp-18-14889-2018, 2018.

699   Kumar, N. K., Corbin, J. C., Bruns, E. A., Massabó, D., Slowik, J. G., Drinovec, L., Močnik, G.,
700   Prati, P., Vlachou, A., Baltensperger, U., Gysel, M., El-Haddad, I., and Prévôt, A. S. H.:
701   Production of particulate brown carbon during atmospheric aging of residential wood-burning
702   emissions, *Atmos. Chem. Phys.*, 18, 17843–17861, https://doi.org/10.5194/acp-18-17843-
703   2018, 2018.

704   Lack, D. A., Moosmüller, H., McMeeking, G. R., Chakrabarty, R. K., and Baumgardner, D.:
705   Characterizing elemental, equivalent black, and refractory black carbon aerosol particles: a
706   review of techniques, their limitations and uncertainties, *Anal. Bioanal. Chem.*, 406, 99–122,
707   https://doi.org/10.1007/s00216-013-7402-3, 2014.

708   Lambe, A. T., Cappa, C. D., Massoli, P., Onasch, T. B., Forestieri, S. D., Martin, A. T., Cummings,
709   M. J., Croasdale, D. R., Brune, W. H., Worsnop, D. R., and Davidovits, P.: Relationship
710   between oxidation level and optical properties of secondary organic aerosol, *Environ. Sci.*
711   *Technol.*, 47, 6349–6357, https://doi.org/10.1021/es401043j, 2013.

712   Laskin, A., Laskin, J., and Nizkorodov, S. A.: Chemistry of atmospheric brown carbon, *Chem. Rev.*,
713   115, 4335–4382, https://doi.org/10.1021/cr5006167, 2015.

714   Li, H. Y., Lamb, K. D., Schwarz, J. P., Selimovic, V., Yokelson, R. J., McMeeking, G. R., and May,
715   A. A.: Inter-comparison of black carbon measurement methods for simulated open biomass
716   burning emissions, *Atmos. Environ.*, 206, 156–169,
717   https://doi.org/10.1016/j.atmosenv.2019.03.010, 2019.

718   Liu, P. F., Abdelmalki, N., Hung, H.-M., Wang, Y., Brune, W. H., and Martin, S. T.: Ultraviolet and
719   visible complex refractive indices of secondary organic material produced by photooxidation
720   of the aromatic compounds toluene and *m*-xylene, *Atmos. Chem. Phys.*, 15, 1435–1446,
721   https://doi.org/10.5194/acp-15-1435-2015, 2015.

722   Liu, J., Lin, P., Laskin, A., Laskin, J., Kathmann, S. M., Wise, M., Caylor, R., Imholt, F., Selimovic,
723   V., and Shilling, J. E.: Optical properties and aging of light-absorbing secondary organic
724   aerosol, *Atmos. Chem. Phys.*, 16, 12815–12827, https://doi.org/10.5194/acp-16-12815-2016,
725   2016a.

726   Liu, X. X., Zhang, Y., Huey, L. G., Yokelson, R. J., Wang, Y., Jimenez, J. L., Campuzano-Jost, P.,
727   Beyersdorf, A. J., Blake, D. R., Choi, Y., St Clair, J. M., Crounse, J. D., Day, D. A., Diskin, G.
728   S., Fried, A., Hall, S. R., Hanisco, T. F., King, L. E., Meinardi, S., Mikoviny, T., Palm, B. B.,
729   Peischl, J., Perring, A. E., Pollack, I. B., Ryerson, T. B., Sachse, G., Schwarz, J. P., Simpson, I.

730   J., Tanner, D. J., Thornhill, K. L., Ullmann, K., Weber, R. J., Wennberg, P. O., Wisthaler, A.,
731   Wolfe, G. M., and Ziemba, L. D.: Agricultural fires in the southeastern U.S. during SEAC4RS:
732   emissions of trace gases and particles and evolution of ozone, reactive nitrogen, and organic
733   aerosol, *J. Geophys. Res. Atmos.*, 121, 7383–7414, https://doi.org/10.1002/2016JD025040,
734   2016b.

735   Liu, J. M., Wang, P. F., Zhang, H. L., Du, Z. Y., Zheng, B., Yu, Q. Q., Zheng, G. J., Ma, Y. L., Zheng,
736   M., Cheng, Y., Zhang, Q., and He, K. B.: Integration of field observation and air quality
737   modeling to characterize Beijing aerosol in different seasons, *Chemosphere*, 242, 125195,
738   https://doi.org/10.1016/j.chemosphere.2019.125195, 2020.

739   Liu, T. Y., Chan, A. W. H., and Abbatt, J. P. D.: Multiphase oxidation of sulfur dioxide in aerosol
740   particles: implications for sulfate formation in polluted environments, *Environ. Sci. Technol.*,
741   8, 4227–4242, https://doi.org/10.1021/acs.est.0c06496, 2021.

742   McClure, C. D., Lim, C. Y., Hagan, D. H., Kroll, J. H., and Cappa, C. D.: Biomass-burning-derived
743   particles from a wide variety of fuels – Part 1: properties of primary particles, *Atmos. Chem.*
744   *Phys.*, 20, 1531–1547, https://doi.org/10.5194/acp-20-1531-2020, 2020.

745   Moosmüller, H., Chakrabarty, R. K., and Arnott, W. P.: Aerosol light absorption and its measurement:
746   a review, *J. Quant. Spectrosc. Radiat. Transf.*, 110, 844–878,
747   https://doi.org/10.1016/j.jqsrt.2009.02.035, 2009.

748   Moteki, N., and Kondo, Y.: Dependence of laser-induced incandescence on physical properties of
749   black carbon aerosols: measurements and theoretical interpretation, *Aerosol Sci. Technol.*, 44,
750   663–675, https://doi.org/10.1080/02786826.2010.484450, 2010.

751   Ning, C. P., Gao, Y., Yu, H. R., Zhang, H. J., Geng, N. B., Cao, R., and Chen, J. P.: FT-ICR mass
752   spectrometry for molecular characterization of water-insoluble organic compounds in winter
753   atmospheric fine particulate matters, *J. Environ. Sci.*, 111, 51–60,
754   https://doi.org/10.1016/j.jes.2020.12.017, 2022.

755   Onasch, T. B., Trimborn, A., Fortner, E. C., Jayne, J. T., Kok, G. L., Williams, L. R., Davidovits, P.,
756   and Worsnop, D. R.: Soot particle aerosol mass spectrometer: development, validation, and
757   initial application, *Aerosol Sci. Technol.*, 46, 804–817,
758   https://doi.org/10.1080/02786826.2012.663948, 2012.

759   Petzold, A., Ogren, J. A., Fiebig, M., Laj, P., Li, S. M., Baltensperger, U., Holzer-Popp, T., Kinne,
760   S., Pappalardo, G., Sugimoto, N., Wehrli, C., Wiedensohler, A., and Zhang, X. Y.:
761   Recommendations for reporting "black carbon" measurements, *Atmos. Chem. Phys.*, 13,
762   8365–8379, https://doi.org/10.5194/acp-13-8365-2013, 2013.

763   Petzold, A., Schloesser, H., Sheridan, P. J., Arnott, W. P., Ogren, J. A., and Virkkula, A.: Evaluation
764   of multiangle absorption photometry for measuring aerosol light absorption, *Aerosol Sci.*
765   *Technol.*, 39, 40–51, https://doi.org/10.1080/027868290901945, 2005.

766   Piazzalunga, A., Bernardoni, V., Fermo, P., Valli, G., and Vecchi, R.: Technical note: On the effect
767   of water-soluble compounds removal on EC quantification by TOT analysis in urban aerosol
768   samples, *Atmos. Chem. Phys.*, 11, 10193–10203, https://doi.org/10.5194/acp-11-10193-2011,

769   2011.

770   Pileci, R. E., Modini, R. L., Bertò, M., Yuan, J., Corbin, J. C., Marinoni, A., Henzing, B., Moerman,
771   M. M., Putaud, J. P., Spindler, G., Wehner, B., Müller, T., Tuch, T., Trentini, A., Zanatta, M.,
772   Baltensperger, U., and Gysel-Beer, M.: Comparison of co-located refractory black carbon (rBC)
773   and elemental carbon (EC) mass concentration measurements during field campaigns at several
774   European sites, *Atmos. Meas. Tech.*, 14, 1379–1403, https://doi.org/10.5194/amt-14-1379-
775   2021, 2021.

776   Samset, B. H., Myhre, G., Herber, A., Kondo, Y., Li, S. M., Moteki, N., Koike, M., Oshima, N.,
777   Schwarz, J. P., Balkanski, Y., Bauer, S. E., Bellouin, N., Berntsen, T. K., Bian, H., Chin, M.,
778   Diehl, T., Easter, R. C., Ghan, S. J., Iversen, T., Kirkevåg, A., Lamarque, J. F., Lin, G., Liu, X.,
779   Penner, J. E., Schulz, M., Seland, Ø., Skeie, R. B., Stier, P., Takemura, T., Tsigaridis, K., and
780   Zhang, K.: Modelled black carbon radiative forcing and atmospheric lifetime in AeroCom
781   Phase II constrained by aircraft observations, *Atmos. Chem. Phys.*, 14, 12465–12477,
782   https://doi.org/10.5194/acp-14-12465-2014, 2014.

783   Schwarz, J. P., Gao, R. S., Fahey, D. W., Thomson, D. S., Watts, L. A., Wilson, J. C., Reeves, J. M.,
784   Darbeheshti, M., Baumgardner, D. G., Kok, G. L., Chung, S. H., Schulz, M., Hendricks, J.,
785   Lauer, A., Karcher, B., Slowik, J. G., Rosenlof, K. H., Thompson, T. L., Langford, A. O.,
786   Loewenstein, M., and Aikin, K. C.: Single-particle measurements of midlatitude black carbon
787   and light-scattering aerosols from the boundary layer to the lower stratosphere, *J. Geophys.*
788   *Res.*, 111, D16207, https://doi.org/10.1029/2006JD007076, 2006.

789   Sharma, S., Leaitch, W. R., Huang, L., Veber, D., Kolonjari, F., Zhang, W., Hanna, S. J., Bertram,
790   A. K., and Ogren, J. A.: An evaluation of three methods for measuring black carbon in Alert,
791   Canada, *Atmos. Chem. Phys.*, 17, 15225–15243, https://doi.org/10.5194/acp-17-15225-2017,
792   2017.

793   State Council: Circular on Further Promoting the Pollution Prevention and Control Battle,
794   https://www.gov.cn/zhengce/2021–11/07/content_5649656.htm, 2021.

795   Stohl, A., Aamaas, B., Amann, M., Baker, L. H., Bellouin, N., Berntsen, T. K., Boucher, O., Cherian,
796   R., Collins, W., Daskalakis, N., Dusinska, M., Eckhardt, S., Fuglestvedt, J. S., Harju, M., Heyes,
797   C., Hodnebrog, Ø., Hao, J., Im, U., Kanakidou, M., Klimont, Z., Kupiainen, K., Law, K. S.,
798   Lund, M. T., Maas, R., MacIntosh, C. R., Myhre, G., Myriokefalitakis, S., Olivié, D., Quaas,
799   J., Quennehen, B., Raut, J. C., Rumbold, S. T., Samset, B. H., Schulz, M., Seland, O., Shine,
800   K. P., Skeie, R. B., Wang, S., Yttri, K. E., and Zhu, T.: Evaluating the climate and air quality
801   impacts of short-lived pollutants, *Atmos. Chem. Phys.*, 15, 10529–10566,
802   https://doi.org/10.5194/acp-15-10529-2015, 2015.

803   Sun, Y. L., He, Y., Kuang, Y., Xu, W. Y., Song, S. J., Ma, N., Tao, J. C., Cheng, P., Wu, C., Su, H.,
804   Cheng, Y. F., Xie, C. H., Chen, C., Lei, L., Qiu, Y. M., Fu, P. Q., Croteau, P., and Worsnop, D.
805   R.: Chemical differences between PM_1 and $PM_{2.5}$ in highly polluted environment and
806   implications in air pollution studies, *Geophys. Res. Lett.*, 47, e2019GL086288,
807   https://doi.org/10.1029/2019GL086288, 2020.

808   Tinorua, S., Denjean, C., Nabat, P., Pont, V., Arnaud, M., Bourrianne, T., Dias Alves, M., and

809   Gardrat, E.: Two-year intercomparison of three methods for measuring black carbon
810   concentration at a high-altitude research station in Europe, *EGUsphere*,
811   https://doi.org/10.5194/egusphere-2024-47, 2024.

812   Uranishi, K., Ikemori, F., Shimadera, H., Kondo, A., and Sugata, S.: Impact of field biomass burning
813   on local pollution and long-range transport of $PM_{2.5}$ in Northeast Asia, *Environ. Pollut.*, 244,
814   414–422, https://doi.org/10.1016/j.envpol.2018.09.061, 2019.

815   Wang, H. C., Lu, K. D., Tan, Z. F., Chen, X. R., Liu, Y. H., and Zhang, Y. H.: Formation mechanism
816   and control strategy for particulate nitrate in China, *J. Environ. Sci.*, 123, 476–486,
817   https://doi.org/10.1016/j.jes.2022.09.019, 2023a.

818   Wang, P. F., Chen, K. Y., Zhu, S. Q., Wang, P., and Zhang, H. L.: Severe air pollution events not
819   avoided by reduced anthropogenic activities during COVID-19 outbreak, *Resour. Conserv.*
820   *Recycl.*, 158, 104814, https://doi.org/10.1016/j.resconrec.2020.104814, 2020.

821   Wang, X., Heald, C. L., Liu, J. M., Weber, R. J., Campuzano-Jost, P., Jimenez, J. L., Schwarz, J. P.,
822   and Perring, A. E.: Exploring the observational constraints on the simulation of brown carbon,
823   *Atmos. Chem. Phys.*, 18, 635–653, https://doi.org/10.5194/acp-18-635-2018, 2018.

824   Wang, Y. T., Zhao, Y., Liu, Y. M., Jiang, Y. Q., Zheng, B., Xing, J., Liu, Y., Wang, S., and Nielsen,
825   C. P.: Sustained emission reductions have restrained the ozone pollution over China, *Nat.*
826   *Geosci.*, 16, 967–974, https://doi.org/10.1038/s41561-023-01284-2, 2023b.

827   Wiedinmyer, C., Akagi, S. K., Yokelson, R. J., Emmons, L. K., Al-Saadi, J. A., Orlando, J. J., and
828   Soja, A. J.: The Fire INventory from NCAR (FINN): a high resolution global model to estimate
829   the emissions from open burning, *Geosci. Model Dev.*, 4, 625–641,
830   https://doi.org/10.5194/gmd-4-625-2011, 2011.

831   Wu, X., Cao, F., Haque, M., Fan, M. Y., Zhang, S. C., and Zhang, Y. L.: Molecular composition and
832   source apportionment of fine organic aerosols in Northeast China, *Atmos. Environ.*, 239,
833   117722, https://doi.org/10.1016/j.atmosenv.2020.117722, 2020.

834   Xiao, Q., Zheng, Y., Geng, G., Chen, C., Huang, X., Che, H., Zhang, X., He, K., and Zhang, Q.:
835   Separating emission and meteorological contributions to long-term $PM_{2.5}$ trends over eastern
836   China during 2000–2018, *Atmos. Chem. Phys.*, 21, 9475–9496, https://doi.org/10.5194/acp-
837   21-9475-2021, 2021.

838   Xie, X. C., Zhang, Y. Z., Liang, R. S., Chen, W., Zhang, P. X., Wang, X., Zhou, Y., Cheng, Y., and
839   Liu, J.M.: Wintertime heavy haze episodes in Northeast China driven by agricultural fire
840   emissions, *Environ. Sci. Technol. Lett.*, 11, 150–157,
841   https://doi.org/10.1021/acs.estlett.3c00940, 2024.

842   Yan, F. P., Kang, S. C., Sillanpää M., Hu, Z. F., Gao, S. P., Chen, P. F., Gautam, S., Reinikainen, S.
843   P., and Li, C. L.: A new method for extraction of methanol-soluble brown carbon: implications
844   for investigation of its light absorption ability, *Environ. Pollut.*, 262, 114300,
845   https://doi.org/10.1016/j.envpol.2020.114300, 2020.

846   Yang, M., Howell, S. G., Zhuang, J., and Huebert, B. J.: Attribution of aerosol light absorption to
847   black carbon, brown carbon, and dust in China - Interpretations of atmospheric measurements

848 during EAST-AIRE, *Atmos. Chem. Phys.*, 9, 2035–2050, https://doi.org/10.5194/acp-9-2035-
849 2009, 2009.

850 Ying, Q, Li, J. Y, and Kota, S. H.: Significant contributions of isoprene to summertime secondary
851 organic aerosol in eastern United States, *Environ. Sci. Technol.*, 49, 7834–7842,
852 https://doi.org/10.1021/acs.est.5b02514, 2019.

853 Zeng, L. H., Dibb, J., Scheuer, E., Katich, J. M., Schwarz, J. P., Bourgeois, I., Peischl, J., Ryerson,
854 T., Warneke, C., Perring, A. E., Diskin, G. S., DiGangi, J. P., Nowak, J. B., Moore, R. H.,
855 Wiggins, E. B., Pagonis, D., Guo, H. Y., Campuzano-Jost, P., Jimenez, J. L., Xu, L., and Weber,
856 R. J.: Characteristics and evolution of brown carbon in western United States wildfires, *Atmos.*
857 *Chem. Phys.*, 22, 8009–8036, https://doi.org/10.5194/acp-22-8009-2022, 2022.

858 Zhang, J., Liu, L., Xu, L., Lin, Q., Zhao, H., Wang, Z., Guo, S., Hu, M., Liu, D., Shi, Z., Huang, D.,
859 and Li, W.: Exploring wintertime regional haze in northeast China: role of coal and biomass
860 burning, *Atmos. Chem. Phys.*, 20, 5355–5372, https://doi.org/10.5194/acp-20-5355-2020,
861 2020.